Chemical Physics Letters 475 (2009) 68–72

Contents lists available at ScienceDirect

Chemical Physics Letters

journal homepage: www.elsevier.com/locate/cplett

Excitation properties of the H3 defect center in diamond: A theoretical study

Chih-Kai Lin [a,*], Huan-Cheng Chang [a], M. Hayashi [b], S.H. Lin [a,c]

[a] Institute of Atomic and Molecular Sciences, Academia Sinica, Taipei, 10617 Taiwan, ROC
[b] Center for Condensed Matter Sciences, National Taiwan University, Taipei, 10617 Taiwan, ROC
[c] Department of Applied Chemistry, National Chiao Tung University, Hsinchu, 30010 Taiwan, ROC

ARTICLE INFO

Article history:
Received 26 March 2009
In final form 6 May 2009
Available online 10 May 2009

ABSTRACT

Theoretical calculations on electronic excitation energies and absorption cross sections of the H3 defect center in diamond were performed. We constructed model clusters with up to 180 atoms to imitate the local environment of the defect center and conducted first-principle calculations. TD-DFT predicted most accurately vertical excitation energy, whereas TD-HF and CIS provided rough estimations for one- and two-photon absorption cross sections. It was found that a model cluster with a diameter larger than ~1.0 nm is required, while relatively low-cost level of theory and basis set are sufficient for characterizing the excitation properties.

1. Introduction

The H3 defect center is the most common optical feature observed for natural diamonds radiation-damaged by high energy particles, followed by thermal annealing [1]. The former creates lattice vacancies (V), which become mobile at temperatures above 500 °C and combined with A aggregates (two adjacent substitutional nitrogen atoms) to form the N–V–N structure with a C_{2v} symmetry [1–4]. The absorption spectra of this center show a zero-phonon line (ZPL) at 2.463 eV (or 503.2 nm), corresponding to the transition between the ground state, $^1A_1$, and the first excited state, $^1B_1$. The phonon side band peaks at ~2.61 eV (or ~475 nm) [2,5–8]. The fluorescence of this transition occurs at ~530 nm with a quantum yield of as high as 0.95 and a lifetime of ~17 ns [6,9,10]. While there is a $^1A_2$ excited state lying just above the $^1B_1$ state, the transition is symmetry-forbidden [1,5]. At annealing temperatures above 1500 °C, some nitrogen aggregates can decompose and release electrons, converting the neutral H3 centers to the negatively charged H2 centers whose ZPL appears at 1.256 eV (or 986.3 nm) [1,6]. The conversion of H2 back to H3 can be achieved by photoionization [11] in a manner similar to that occurring between NV^- and NV^0 [12,13].

A previous study has measured the one-photon absorption (OPA) cross section of the $^1A_1 \rightarrow {}^1B_1$ transition to be 1.4×10^{-17} cm^2 under 488 nm excitation using an Ar^+ laser [8]. More recently, our group recorded a similar value of $\sigma_{OPA} = (1.7 \pm 0.5) \times 10^{-17}$ cm^2 at 488 nm as well as $(2.1 \pm 0.5) \times 10^{-17}$ cm^2 at 473 nm [14]. While there have been many experimental measurements concerning this defect center, the corresponding theoretical explorations are quite few. Several studies have examined the stability of the H3 center using either semi-empirical or local density functional approaches [15,16], but so far a detailed computational characterization of the defect structure as well as its excitation properties is still absent. In this work, we present first-principle investigations on this defect center with the aid of molecular cluster models that have been proven reliable in previous works [17,18].

2. Computational methods

In order to calculate the excitation properties of the H3 defect center, the methodology developed in our previous study on the NV^- defect center [17] has been applied. First of all, several finite-sized diamond lattice (large diamondoid) molecular cluster models were constructed to imitate the local environment of the defect center. The smallest one was $C_{48}(NVN)H_{52}$, where two nitrogen atoms and one vacancy were enclosed by 48 carbon atoms and the surface was passivated by hydrogen atoms. Increasing the number of carbon shells around the defect center $C_{84}(NVN)H_{76}$, $C_{103}(NVN)H_{86}$, and $C_{178}(NVN)H_{116}$ were obtained, which have spherical or ellipsoidal conformations (Fig. 1). These structures were then optimized either by the Hartree–Fock algorithm (HF) or by the density functional theory (DFT) with the B3LYP functional. Following the ground state geometry optimization, time-dependent methods including TD-HF and TD-DFT as well as configuration interaction singles (CIS) were applied to search electronic vertical excitation energies and transition dipole moments. The commonly used Pople basis set 6-31G(d) was chosen, and 6-31 + G(d) was additionally tested in several cases to check the influence of the diffuse function. Dunning's correlation consistent basis set cc-pVDZ was applied as well for comparison. All these computations were done by using the GAUSSIAN 03 package [19].

* Corresponding author. Fax: +886 2 2362 0200.
E-mail address: ethene@gate.sinica.edu.tw (C.-K. Lin).

0009-2614/$ - see front matter © 2009 Elsevier B.V. All rights reserved.
doi:10.1016/j.cplett.2009.05.011

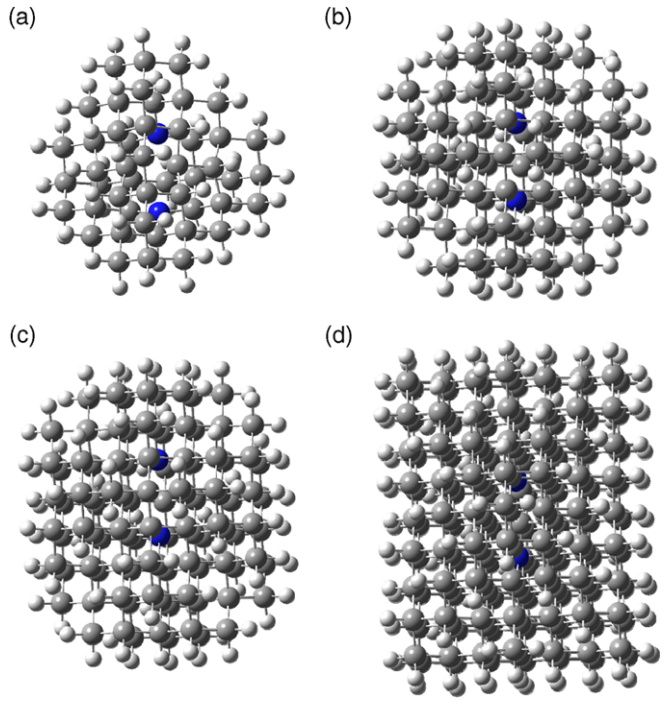

Fig. 1. Model clusters mimicking the local environment of the H3 defect center in diamond: (a) $C_{48}(NVN)H_{52}$ (C_{2v}); (b) $C_{84}(NVN)H_{76}$ (C_{2v}); (c) $C_{103}(NVN)H_{86}$ (C_s); (d) $C_{178}(NVN)H_{116}$ (C_{2v}). Each model cluster contains two nitrogen atoms and one vacancy in its center, and is surface-passivated with hydrogen atoms.

The absorption cross sections could be calculated as soon as the information of excitation properties was computed. According to the derivations based on the Fermi golden rule, the one-photon absorption (OPA) cross section in atomic units is [17,20]

$$\sigma_{\mathrm{OPA}}(\omega) = \frac{4\pi^2\alpha\omega}{3n_e(\omega)}|\mathbf{R}_{fi}|^2 \sum_{v}\sum_{v'} P_{iv}|\langle\Theta_{fv'}|\Theta_{iv}\rangle|^2 D(\omega_{fv',iv}-\omega,\gamma_{fv',iv}), \tag{1}$$

where iv and fv' refer to the initial and final electronic states i and f with vibrational quantum numbers v and v', respectively; ω is the pumping energy (expressed as angular frequency); $\omega_{fv',iv}$ is the energy gap between the two vibronic states; $\alpha = 7.297\times10^{-3}$ is the fine structure constant; n_e is the refractive index; $\mathbf{R}_{fi}$ is the transition dipole moment depicted as a spatial vector. The distribution function, i.e. the summation over products of Boltzmann distribution of the initial state P_{iv}, the Franck–Condon factor $|\langle\Theta_{fv'}|\Theta_{iv}\rangle|^2$, and the Lorentzian lineshape function $D(\Delta\omega,\gamma)$ corresponding to each vibronic transition, could be deduced by empirical potential energy surface models or by fitting the shape of experimental spectra [21]. At low temperature, all the initial population readily resides in the $v=0$ level and Eq. (1) can be approximated as

$$\sigma_{\mathrm{OPA}}(\omega) = \frac{4\pi^2\alpha\omega}{3n_e(\omega)}|\mathbf{R}_{fi}|^2 \sum_{v'}|\langle\Theta_{fv'}|\Theta_{i0}\rangle|^2 D(\omega_{fv',i0}-\omega,\gamma_{fv',i0}). \tag{2}$$

On the other hand, the two-photon absorption (TPA) cross section, with a single incident beam and the low temperature condition, is [17,22]

$$\sigma_{\mathrm{TPA,linear}}(\omega,\omega) = \frac{4\pi^3\alpha^2\omega^2}{15n_e^2(\omega)}\sum_{a}^{x,y,z}\sum_{b}^{x,y,z}(S_{fi}^{aa}S_{fi}^{bb*}+2S_{fi}^{ab}S_{fi}^{ab*}) \times\sum_{v'}|\langle\Theta_{fv'}|\Theta_{i0}\rangle|^2 D(\omega_{fv',i0}-2\omega,\gamma_{fv',i0}) \tag{3}$$

for linearly polarized incident field, and

$$\sigma_{\mathrm{TPA,circular}}(\omega,\omega) = \frac{4\pi^3\alpha^2\omega^2}{15n_e^2(\omega)}\sum_{a}^{x,y,z}\sum_{b}^{x,y,z}(-S_{fi}^{aa}S_{fi}^{bb*}+3S_{fi}^{ab}S_{fi}^{ab*}) \times\sum_{v'}|\langle\Theta_{fv'}|\Theta_{i0}\rangle|^2 D(\omega_{fv',i0}-2\omega,\gamma_{fv',i0}) \tag{4}$$

for circularly polarized incident field, where

$$S_{fi}^{ba}(\omega,\omega) = \sum_{m}\left(\frac{R_{fm}^{b}R_{mi}^{a}}{\omega_{mi}-\omega}+\frac{R_{fm}^{a}R_{mi}^{b}}{\omega_{mi}-\omega}\right) \tag{5}$$

is the two-photon transition matrix element related to transition dipole moments involving the intermediate electronic state m; a and b refer to molecular coordinates x, y, or z; R^a represents the a-component of the transition dipole moment. It is noticed that the intermediate state m counts for all virtual states as well as the initial and final states for non-centrosymmetric systems [23–25].

3. Results and discussion

3.1. Vertical excitation energies

At the end of the optimization process for the ground state, all models achieved the totally symmetric term ($^1A_1$ in the C_{2v} point group or $^1A'$ state in the C_s point group), independent of level of theory or basis set used. The first excited state was found to be $^1B_1$ in larger model clusters (with 84 or more carbon atoms) with a $^1A_2$ state appearing in its vicinity. Table 1 lists the computational results for the first three excited states, and Fig. 2 illustrates the vertical excitation energies from the ground state to the first $^1B_1$ excited states, obtained at different cluster sizes and different levels of computation. It is noticed that the cc-pVDZ basis set yielded virtually the same results as the 6-31G(d) one, e.g. the calculated excitation energy differed by only ~1%, hence the results are omitted from the table.

The vertical excitation energy to the first excited state, ΔE, as measured experimentally can be best reproduced by TD-DFT calculation for larger models, similar to our previous finding for the NV^- center [17]. The value computed for the largest model cluster (178 carbon atoms) was 2.77 eV, which compares satisfactorily with the experimental absorption maximum of (2.61 ± 0.10) eV. At this level of theory, the second excited state, $^1A_2$, to which the transition from the ground state is symmetry-forbidden, was predicted to lie above $^1B_1$ by ~0.05 eV, which is in a good agreement with experimentally reported values [1,5]. Examining the molecular orbitals (MOs, demonstrated in Fig. 3) and the configuration-interaction expansion coefficients of these transitions suggests that the HOMO (a_1) → LUMO (b_1) transition plays a leading role in the $^1A_1 \rightarrow {}^1B_1$ excitation, and the HOMO−1 (b_2) → LUMO (b_1) transition participates mostly in the $^1A_1 \rightarrow {}^1A_2$ excitation. The two occupied MOs mentioned here are nearly degenerate, resulting in the nearly degenerate excited states.

Comparisons of the TD-DFT result with those of TD-HF and CIS in Table 1 shows that the vertical excitation energies calculated with the latter two methods are significantly overestimated. The reason for this discrepancy clearly is associated with the fact that the Kohn–Sham formalism evaluates the energies of virtual MOs more accurately than the HF algorithm [26]. On the other hand, it is noted that the introduction of diffuse functions into the basis sets has only a minor effect on the calculations with larger cluster models, because these clusters are large enough to avoid the interference from surface atoms and to prevent electron densities leaking out of the defect center. The 'threshold' of this cluster size effect is about 84 carbon atoms, corresponding to a diameter of ~1.0 nm, in both NV^- and H3 cases.

Table 1
Calculated symmetries,[a] vertical excitation energies ΔE (eV), and magnitudes of the transition dipole moments $|\boldsymbol{\mu}|$ (debye) of the first three excited states associated with the H3 defect centers in diamond model clusters.

Model (conformation)	Level of theory	Basis set[b]	First excited state			Second excited state			Third excited state		
			Term	ΔE (eV)	$\|\boldsymbol{\mu}\|$ (D)	Term	ΔE (eV)	$\|\boldsymbol{\mu}\|$ (D)	Term	ΔE (eV)	$\|\boldsymbol{\mu}\|$ (D)
$C_{48}(NVN)H_{52}$ (tetrahedron)	CIS	6-31G(d)	$^1B_1$	8.362	2.372	$^1B_2$	9.339	1.818	$^1A_2$	9.355	0.000
		6-31 + G(d)	$^1B_2$	6.587	2.483	$^1A_1$	6.628	1.837	$^1B_1$	7.085	1.819
	TD-HF	6-31G(d)	$^1B_1$	8.207	2.257	$^1B_2$	9.293	1.657	$^1A_1$	9.322	1.363
		6-31 + G(d)	$^1B_2$	6.566	2.321	$^1A_1$	6.604	1.706	$^1B_1$	7.055	1.767
	TD-DFT	6-31G(d)	$^1A_2$	4.692	0.000	$^1B_1$	4.830	0.984	$^1B_2$	5.846	0.941
		6-31 + G(d)	$^1A_2$	4.071	0.000	$^1A_1$	4.094	1.317	$^1B_1$	4.101	1.307
$C_{84}(NVN)H_{76}$ (sphere)	CIS	6-31G(d)	$^1B_1$	6.021	3.650	$^1A_2$	7.573	0.000	$^1B_1$	8.188	2.077
		6-31 + G(d)	$^1B_1$	5.943	3.293	$^1A_1$	6.112	0.462	$^1B_2$	6.192	0.875
	TD-HF	6-31G(d)	$^1B_1$	5.695	3.361	$^1A_2$	7.561	0.000	$^1B_1$	8.108	1.815
		6-31 + G(d)	$^1B_1$	5.643	3.269	$^1A_1$	6.110	0.460	$^1B_2$	6.188	0.841
	TD-DFT	6-31G(d)	$^1B_1$	2.970	2.112	$^1A_2$	2.975	0.000	$^1A_1$	4.693	0.071
		6-31 + G(d)	$^1B_1$	2.891	1.886	$^1A_2$	2.941	0.000	$^1A_1$	2.994	0.109
$C_{103}(NVN)H_{86}$ (sphere)	CIS	6-31G(d)	$^1A''$	6.046	3.490	$^1A''$	7.561	0.079	$^1A''$	8.184	2.008
		6-31 + G(d)	$^1A''$	5.960	3.052	$^1A'$	6.111	0.535	$^1A'$	6.221	0.594
	TD-HF	6-31G(d)	$^1A''$	5.724	3.193	$^1A''$	7.549	0.071	$^1A''$	8.103	1.757
		6-31 + G(d)	$^1A''$	5.667	3.071	$^1A'$	6.109	0.526	$^1A'$	6.218	0.562
	TD-DFT	6-31G(d)	$^1A''$	2.961	1.195	$^1A''$	2.999	1.576	$^1A'$	4.640	0.186
		6-31 + G(d)	$^1A''$	2.893	1.596	$^1A''$	2.947	0.587	$^1A'$	2.987	0.145
$C_{178}(NVN)H_{116}$ (ellipsoid)	CIS	6-31G(d)	$^1B_1$	5.787	3.208	$^1A_2$	7.304	0.000	$^1B_1$	7.999	1.543
	TD-HF	6-31G(d)	$^1B_1$	5.450	2.832	$^1A_2$	7.291	0.000	$^1B_1$	7.923	1.327
	TD-DFT	6-31G(d)	$^1B_1$	2.767	1.873	$^1A_2$	2.809	0.000	$^1B_1$	4.423	0.280
Expt.[c]			$^1B_1$	2.61	–	$^1A_2$	2.63	–	–	–	–

[a] The ground state is totally symmetric, i.e. $^1A_1$ or $^1A'$.
[b] The cc-pVDZ basis set yields virtually the same results as the 6-31G(d) one.
[c] Refs. [5,7].

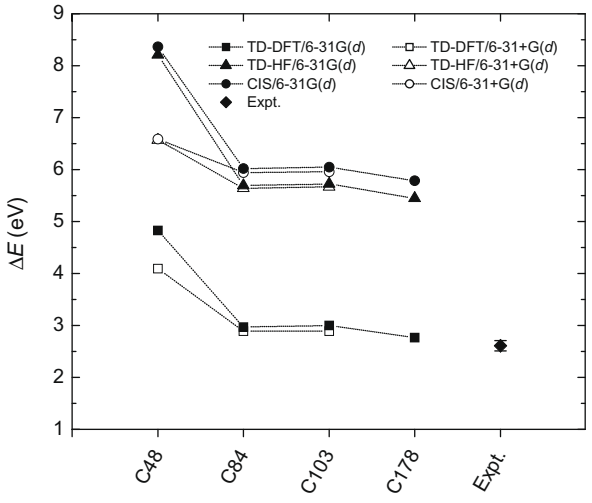

Fig. 2. Calculated vertical excitation energies from the ground state ($^1A_1$ or $^1A'$) to the first excited state ($^1B_1$ or $^1A''$) of the H3 defect center in diamond. The experimental value is (2.61 ± 0.10) eV [3,5].

3.2. One- and two-photon absorption cross sections

According to Eq. (2) the OPA cross sections of the H3 defect center with current model clusters have been calculated. The distribution function was approximated ~57 au at the excitation wavelength of 473 nm (or 2.62 eV, corresponding to the absorption maximum) by fitting the absorption spectral curve reported in Ref. [6]. The refractive index n_e = 2.439 at this wavelength has been reported [1]. With the computed information of vertical excitation energies and transition dipole moments, σ_{OPA} values of transitions from the ground state to the first $^1B_1$ excited state were carried out as tabulated in Table 2 and illustrated in Fig. 4.

The calculated results of the H3 center showed the same trend as those in the NV^- case that TD-DFT severely underestimated the OPA cross sections by a factor of about 4–5, probably due to undervaluing the transition dipole moments. The CIS and TD-HF values, $(2.59 \pm 0.28) \times 10^{-17}$ cm^2 and $(2.02 \pm 0.29) \times 10^{-17}$ cm^2, respectively, were in good agreement with the experimental data, $(2.1 \pm 0.5) \times 10^{-17}$ cm^2, measured under the 473 nm excitation [14]. However, the agreement was rather coincident because the latter two methods overestimated the vertical excitation energies as twice the experimental value (Fig. 2) and therefore raised the OPA cross sections [cf. Eq. (2)]. If the vertical excitation energy had been calculated correctly, σ_{OPA} obtained from CIS and TD-HF should also be somewhat underestimated, similar to that occurred in the NV^- case [17].

The TPA cross section of the H3 center, on the other hand, has not been measured experimentally so far. In a previous study of the NV^- center, the authors applied in the TPA process just twice the excitation wavelength of the OPA measurements, hence keeping the same total pumping energy [27]. In the present H3 center case, however, there is no suitable laser light source fitting this condition (i.e. ω_{TPA} = 946 nm when ω_{OPA} = 473 nm). Nevertheless, we could roughly predict σ_{TPA} with the aid of CIS calculation which provides necessary information of transition dipole moments between excited states. It has been known that although CIS presents systematic deviation in computed results, by error cancellation it could still estimate absorption cross sections to the correct order of magnitude [17]. Obtaining vertical excitation energies and transition dipole moments of the first several states from computation, σ_{TPA} at the '946 nm' excitation was deduced using Eqs. (3)–(5).

Due to the selection rule in the C_{2v} point group, the symmetry-allowed two-photon process between the ground state ($^1A_1$) and the first excited state ($^1B_1$) requires an intermediate state of either $^1A_1$ or $^1B_1$. Examining these possible virtual states, however, we found the calculated transition dipole moments were typically much less than 1 au (2.54 debye), yielding small values of transition matrix elements from Eq. (5). As a result, σ_{TPA} of the $^1A_1 \rightarrow {}^1B_1$ excitation was predicted to be a negligible value, $\sim 1.0 \times 10^{-53}$ cm^4 s (~0.001 GM) per photon. On the other hand,

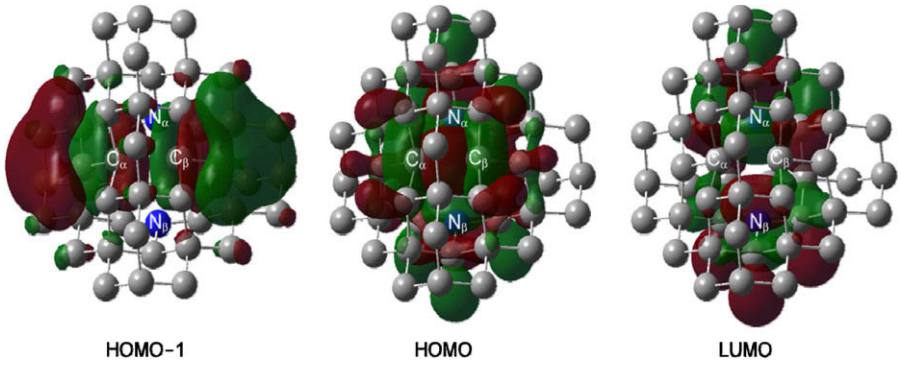

Fig. 3. Molecular orbital maps of HOMO−1, HOMO, and LUMO, calculated for $C_{48}(NVN)H_{52}$ by B3LYP/6-31G(d). In the structures superimposed on the orbital maps, the vacancy is surrounded by two nitrogen atoms (labeled as N_α and N_β) and two carbon atoms (labeled as C_α and C_β), and surface hydrogen atoms are not shown for simplicity.

Table 2
Calculated vertical excitation energy ΔE, magnitude of the transition dipole moment $|\boldsymbol{\mu}|$, oscillator strength f, CI expansion coefficient of the HOMO → LUMO transition $a_{H\to L}$, and one-photon absorption cross section σ_{OPA} of the $^1A_1 \to {}^1B_1$ (or $^1A' \to {}^1A'$) transition associated with the H3 defect centers in diamond model clusters.

Model (conformation)	Level of theory	Basis set[a]	ΔE (eV)	$\|\boldsymbol{\mu}\|$ (debye)	f	$a_{H\to L}$	σ_{OPA}[b] (10^{-17} cm^2)
$C_{48}(NVN)H_{52}$ (tetrahedron)	CIS	6-31G(d)	8.362	2.372	0.1785	0.556	1.700
		6-31 + G(d)	6.587	2.483	0.0890	–[c]	2.237
	TD-HF	6-31G(d)	8.207	2.257	0.1584	0.538	1.508
		6-31 + G(d)	7.055	1.767	0.0835	–	1.937
	TD-DFT	6-31G(d)	4.830	0.984	0.0177	0.684	0.169
		6-31 + G(d)	4.101	1.307	0.0265	0.694	0.858
$C_{84}(NVN)H_{76}$ (sphere)	CIS	6-31G(d)	6.021	3.650	0.3040	0.642	2.896
		6-31 + G(d)	5.943	3.293	0.2448	–	2.354
	TD-HF	6-31G(d)	5.695	3.361	0.2438	0.625	2.322
		6-31 + G(d)	5.643	3.269	0.2285	–	2.181
	TD-DFT	6-31G(d)	2.970	2.112	0.0502	0.612	0.479
		6-31 + G(d)	2.891	1.886	0.0390	0.626	0.372
$C_{103}(NVN)H_{86}$ (sphere)	CIS	6-31G(d)	6.046	3.490	0.2791	0.631	2.659
		6-31 + G(d)	5.960	3.052	0.2105	–	2.037
	TD-HF	6-31G(d)	5.724	3.193	0.2213	0.613	2.108
		6-31 + G(d)	5.667	3.071	0.2028	–	1.932
	TD-DFT	6-31G(d)	2.999	1.576	0.0283	0.467	0.394
		6-31 + G(d)	2.893	1.596	0.0279	0.604	0.301
$C_{178}(NVN)H_{116}$ (ellipsoid)	CIS	6-31G(d)	5.787	3.208	0.2257	0.645	2.150
	TD-HF	6-31G(d)	5.450	2.832	0.1657	0.628	1.579
	TD-DFT	6-31G(d)	2.767	1.873	0.0368	0.611	0.352
Average[d]	CIS	6-31G(d)	5.95 ± 0.11	3.45 ± 0.16		–	2.57 ± 0.28
	TD-HF	6-31G(d)	5.62 ± 0.12	3.13 ± 0.20		–	2.00 ± 0.28
	TD-DFT	6-31G(d)	2.91 ± 0.10	1.85 ± 0.19		–	0.41 ± 0.05
Expt.[e]			2.61 ± 0.10	–		–	2.1 ± 0.5

[a] The cc-pVDZ basis set yields virtually the same results as the 6-31G(d) one.
[b] Values at the absorption maxima.
[c] Apparent divergence due to discrepant arrangement of molecular orbitals.
[d] Averages calculated for the largest three model clusters.
[e] Refs. [5,7].

the excitation to the second excited state ($^1A_2$) should also be considered because of its vicinity in energy. The $^1A_1 \to {}^1A_2$ transition is symmetry-forbidden in the one-photon process but allowed in the two-photon process via a $^1B_1$ or a $^1B_2$ intermediate state. The calculated values were much larger than the former transition but yet minute, that is, $\sim 3.0 \times 10^{-52}$ cm^4 s per photon or $\sim 4.5 \times 10^{-52}$ cm^4 s per photon under linearly or circularly polarized incident field, respectively. Concluding these findings, while the OPA cross section approaches its maximum at 473 nm, the TPA process with the same total excitation energy is quite weak, suggesting a very hard experimental observation.

4. Summary

The procedure developed in the theoretical studies on the diamond NV^- defect center could be duplicated well in the case of the H3 defect center, which has the N–V–N structure in the C_{2v} point group with the neutral charge state. Establishing model clusters up to 178 carbon and 2 nitrogen atoms, we successfully reproduced the vertical excitation energy from the ground state ($^1A_1$) to the first excited state ($^1B_1$), together with locating the nearby second excited state ($^1A_2$) to which the transition from the ground state is symmetry-forbidden, using TD-DFT computations with the B3LYP functional and the 6-31G(d) basis set. CIS and TD-HF, on the other hand, showed the one-photon absorption cross sections relatively close to experimental measurements. CIS further predicted very small two-photon absorption cross sections at the total excitation energy corresponding to the one-photon absorption maximum, awaiting experimental verification. These achievements promised further computational investigations on other defect centers in diamond.

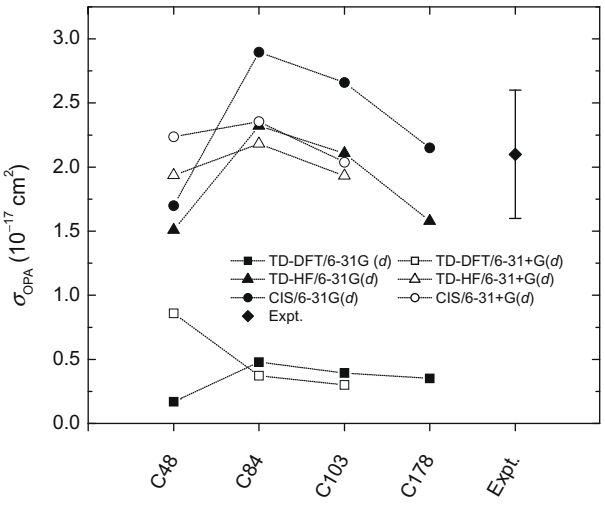

Fig. 4. Calculated OPA cross sections of the $^1A_1 \rightarrow {}^1B_1$ (or $^1A' \rightarrow {}^1A''$) transition of the H3 defect center in diamond at its absorption maximum. The experimental value at 473 nm (or 2.62 eV) is $(2.1 \pm 0.5) \times 10^{-17}$ cm^2 [14].

References

[1] A.M. Zaitsev, Optical Properties of Diamond, Springer-Verlag, Berlin, 2001.
[2] G. Davies, J. Phys. C 7 (1974) 3797.
[3] G. Davies, J. Phys. C 9 (1976) L537.
[4] G. Davies, N.B. Manson, in: G. Davies (Ed.), Properties and Growth of Diamond, EMIS Datareviews Series No. 9, INSPEC, the Institute of Electrical Engineers, London, 1994, p. 173.
[5] A.T. Collins, H. Kanda, H. Kitawaki, Diamond Relat. Mater. 9 (2000) 113.
[6] S.C. Rand, L.G. DeShazer, Opt. Lett. 10 (1985) 481.
[7] A.T. Collins, A. Connor, C.-H. Ly, A. Sheraaf, P.M. Spear, J. Appl. Phys. 97 (2005) 083517.
[8] W.T. Roberts, S.C. Rand, S. Redmond, NASA Tech Briefs NPO-30796, 2005.
[9] S.C. Rand, in: G. Davies (Ed.), Properties and Growth of Diamond, EMIS Datareviews Series No. 9, INSPEC, The Institute of Electrical Engineers, London, 1994, p. 235.
[10] M.D. Crossfield, G. Davies, A.T. Collins, E.C. Lightowlers, J. Phys. C 7 (1974) 1909.
[11] Y. Mita, Y. Nisida, K. Suito, A. Onodera, S. Yazu, J. Phys.: Condens. Mater. 2 (1990) 8567.
[12] K. Iakoubovskii, G.J. Adriaenssens, M. Nesladek, J. Phys.: Condens. Mater. 12 (2000) 189.
[13] T. Gaebel et al., Appl. Phys. B 82 (2006) 243.
[14] T.-L. Wee, Y.-W. Mau, C.-Y. Fang, H.-L. Hsu, C.-C. Han, C.-H. Chang, Diamond Relat. Mater. 18 (2009) 567.
[15] A. Mainwood, Phys. Rev. B 49 (1994) 7934.
[16] R. Jones, Mater. Sci. Forum 143–147 (1994) 45.
[17] C.-K. Lin, Y.-H. Wang, H.-C. Chang, M. Hayashi, S.H. Lin, J. Chem. Phys. 129 (2008) 124714.
[18] J.A. Larsson, P. Delaney, Phys. Rev. B 77 (2008) 165201.
[19] M.J. Frisch et al., Gaussian 03, Revision C.2, Gaussian, Inc., Pittsburgh, PA, 2003.
[20] K.K. Liang, R. Chang, M. Hayashi, S.H. Lin, Principle of Molecular Spectroscopy and Photochemistry, National Chung-Hsing University Press, Taichung, 2001.
[21] C.-K. Lin, H.-C. Chang, S.H. Lin, J. Phys. Chem. A 111 (2007) 9347.
[22] S.H. Lin, Y. Fujimura, H.J. Neusser, E.W. Schlag, Multiphoton Spectroscopy of Molecules, Academic Press, New York, 1984.
[23] B. Dick, G. Hohlneicher, J. Chem. Phys. 76 (1982) 5755.
[24] W.J. Meath, E.A. Power, J. Phys. B 17 (1984) 763.
[25] B.N. Jagatap, W.J. Meath, J. Opt. Soc. Am. B 19 (2002) 2673.
[26] A. Dreuw, M. Head-Gordon, Chem. Rev. 105 (2005) 4009.
[27] T.-L. Wee et al., J. Phys. Chem. A 111 (2007) 9379.